

# PoP-Net: Pose over Parts Network for Multi-Person 3D Pose Estimation from a Depth Image

Yuliang Guo<sup>\*</sup>, Zhong Li<sup>†</sup>, Zekun Li<sup>‡</sup>, Xiangyu Du, Shuxue Quan, Yi Xu

OPPO US Research Center

{yuliang.guo, zhong.li, zekun.li, xiangyu.du, shuxue.quan, yi.xu}@oppo.com

## Abstract

In this paper, a real-time method called PoP-Net is proposed to predict multi-person 3D poses from a depth image. PoP-Net learns to predict bottom-up part detection maps and top-down global poses in a single-shot framework. A simple and effective fusion process is applied to fuse the global poses and part detection. Specifically, a new part-level representation, called Truncated Part Displacement Field (TPDF), is introduced. It drags low-precision global poses towards more accurate part locations while maintaining the advantage of global poses in handling severe occlusion and truncation cases. A mode selection scheme is developed to automatically resolve the conflict between global poses and local detection. Finally, due to the lack of high-quality depth datasets for developing and evaluating multi-person 3D pose estimation methods, a comprehensive depth dataset with 3D pose labels is released. The dataset is designed to enable effective multi-person and background data augmentation such that the developed models are more generalizable towards uncontrolled real-world multi-person scenarios. We show that PoP-Net has significant advantages in efficiency for multi-person processing and achieves the state-of-the-art results both on the released challenging dataset and on the widely used ITOP dataset [Haque *et al.*, 2016].

## 1 Introduction

Human pose estimation plays an important role in a wide variety of applications, and there is a rich pool of literature for human pose estimation methods. Categorizations of existing methods can be made from different dimensions. There are methods mostly relying on a single image to predict human poses [Tekin *et al.*, 2016; Pavlakos *et al.*, 2017; Mehta *et al.*, 2017; Omran *et al.*, 2018; Kanazawa *et al.*, 2018] and others based on multiple cameras [Rhodin *et al.*, 2016;

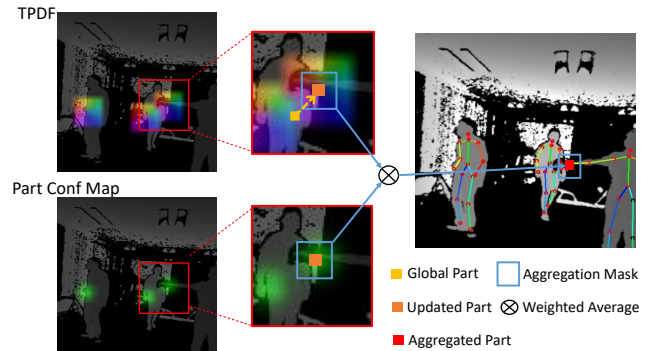


Figure 1: **Our paradigm.** Part representations and global poses predicted from PoP-Net can be explicitly fused via utilizing Truncated-Part-Displacement-Field (TPDF). A part from global pose is dragged towards more precise bottom-up part position following a displacement vector. More reliable part position is estimated via a part-confidence-weighted average of TPDF within the aggregation mask.

Elhayek *et al.*, 2017]. Some methods are capable of predicting multiple poses [Cao *et al.*, 2017; Mehta *et al.*, 2018; Zanfiri *et al.*, 2018; Mehta *et al.*, 2019; Rogez *et al.*, 2020] while others are focusing on single person [Wei *et al.*, 2016; Newell *et al.*, 2016; Pavlakos *et al.*, 2017]. Some methods estimate 3D poses [Zhou *et al.*, 2017; Martinez *et al.*, 2017; Pavlakos *et al.*, 2018; Xiong *et al.*, 2019] while others only predict 2D poses [Wei *et al.*, 2016; Newell *et al.*, 2016; Papandreou *et al.*, 2017; Fang *et al.*, 2017]. Methods can also be differentiated by inputs, while most methods use RGB images [Cao *et al.*, 2017; Papandreou *et al.*, 2017; Mehta *et al.*, 2017; Mehta *et al.*, 2019], others use depth maps [Martínez-González *et al.*, 2018; Wang *et al.*, 2016; Xiong *et al.*, 2019]. This paper focuses on real-time and multi-person 3D human pose estimation from a depth image.

In the era of deep learning, a large pool of Deep Neural Networks (DNN)-based methods [Wei *et al.*, 2016; Newell *et al.*, 2016; Pishchulin *et al.*, 2016; Cao *et al.*, 2017; He *et al.*, 2017; Papandreou *et al.*, 2017; Xiong *et al.*, 2019] have been developed for multi-person pose estimation. Ideas from existing literature can be generally categorized into three prototypical trends. The simplest idea is to directly extend a single shot object detector [Liu *et al.*, 2016;

<sup>\*</sup>Contact Author

<sup>†</sup>Contact Author

<sup>‡</sup>The work was done when Li was an intern with OPPO

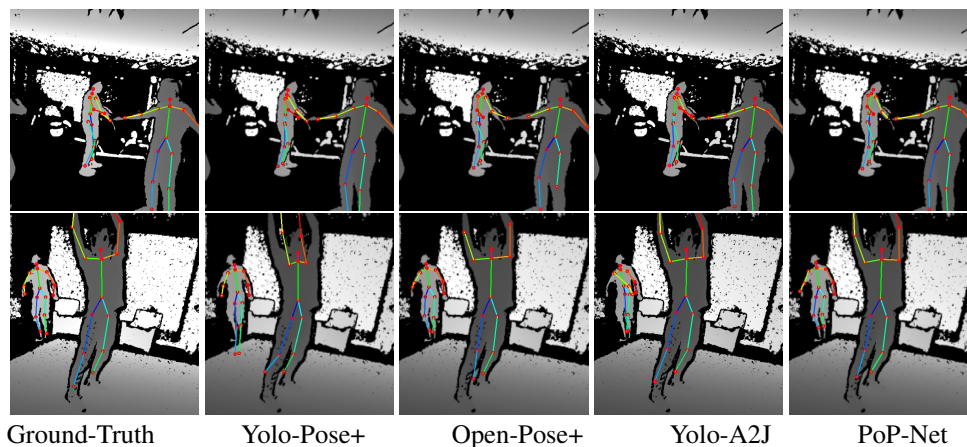


Figure 2: **Visual comparison of prototypical methods:** methods are compared on two examples from KD3DH testing set.

Redmon *et al.*, 2016; Redmon and Farhadi, 2017] with additional pose attributes, so that the network can output human poses. Such single-shot regression can be super efficient, but has low part accuracy because a long-range inference for part locations is involved by using a center-relative pose representation as shown in Figure 2 (Yolo-Pose+). The second one is to make a two-stage pipeline that the first stage detects object bounding boxes, and the second stage estimates pose within them [Papandreou *et al.*, 2017; He *et al.*, 2017; Xiong *et al.*, 2019]. Two-stage methods can be very accurate, as shown in Figure 2 (Yolo-A2J), but not as efficient when more human beings appear in an image. In addition, more sophisticated work is required to solve the compatibility issue between pose estimation and bounding box detection [He *et al.*, 2017; Redmon *et al.*, 2016]. The third idea is to detect human poses from part<sup>1</sup> association [Iqbal and Gall, 2016; Newell *et al.*, 2017; Cao *et al.*, 2017; Martínez-González *et al.*, 2018; Mehta *et al.*, 2019]. Although part detection can be rather efficient, solving the part association problem is usually time consuming. OpenPose [Cao *et al.*, 2017] gained its popularity for introducing an efficient solution to solve this problem, resulting in a network benefiting from both the single shot for high efficiency and the part-based dense representation for high positional precision. However, a pure bottom-up method does not infer pose in a global sense, so it is rather sensitive to occlusion, truncation, and ambiguities in symmetric limbs (Figure 2 OpenPose+). Moreover, dependency on the bipartite matching in assembling parts prevents combining this method with a global-pose<sup>2</sup> network towards an end-to-end solution.

Extending a well-established pipeline for multi-person 2D poses from an RGB image [Papandreou *et al.*, 2017; Ren *et al.*, 2017; Cao *et al.*, 2017] to a depth image-based 3D pose estimation is straightforward because 3D information is partially available from the input [Haque *et al.*, 2016; Xiong *et al.*, 2019]. Additional designs of the network only need to focus on denoising the raw depth input and estimating

the true depth under occlusion. The resulting network does not involve much novel design compared to the network aiming to recover 3D information from an RGB image [Mehta *et al.*, 2017; Mehta *et al.*, 2018; Mehta *et al.*, 2019]. Consequently, the majority of the effort in our work has been spent on delivering accurate estimation of multiple 2D poses and the fusion of available depth information from different components.

In this paper, we present a method called Pose-over-Parts Network (**PoP-Net**) to estimate multiple 3D poses from a depth image. As illustrated in Figure 1, the main idea of PoP-Net is to fuse the predicted bottom-up parts and top-down global poses explicitly. This fusion process is enabled by a new intermediate representation, called Truncated-Part-Displacement-Field (TPDF), which is a vector field that records the vector pointing to the closest part location at every 2D position. TPDF is utilized to drag a structural valid global pose towards more positional precise part detection, such that the advantages from global pose and local part detection can be naturally unified.

Although there are a decent amount of RGB datasets [Lin *et al.*, 2014; Ionescu *et al.*, 2014; Andriluka *et al.*, 2014] in the prior art, there are limited high-quality depth datasets for multi-person 3D pose for depth images. In this paper, we release a comprehensive dataset covering most essential aspects of visual variance related to 3D human pose estimation. The dataset facilitates training models that can be generalized to novel background and unobserved multi-person configurations in real-world applications.

The contribution of this paper is four fold. First, we introduce an efficient framework that predicts multiple 3D poses in one shot. Second, we propose a new part-level representation TPDF, which enables an explicit fusion of global poses and part-level representations. Third, we introduce a mode selection scheme that automatically resolve the possible conflicts between local and global predictions. Finally, we introduce a comprehensive depth image-based 3D human pose dataset to facilitate the development of models applicable to real-world multi-person challenges.

<sup>1</sup>The definitions of ‘part’ and ‘joint’ are interchangeable.

<sup>2</sup>The extension from an one-shot detection network is considered a global pose network.

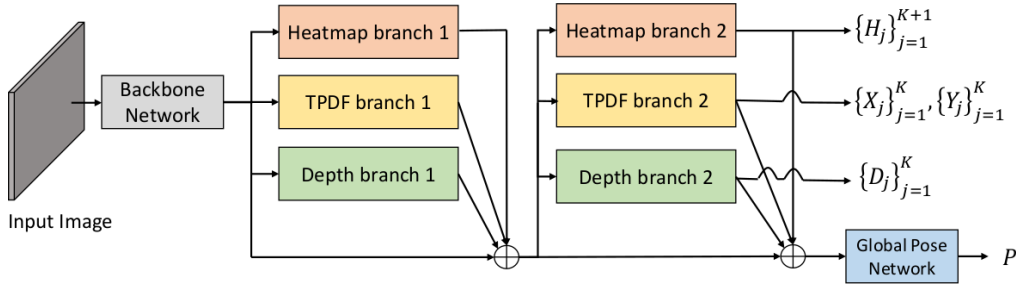


Figure 3: **PoP-Net** is composed of a backbone network, three functional branches, and a global pose network. The functional branches are organized in two stages with split and merge. PoP-Net outputs three part-level maps and a global pose map.

## 2 Prior-over-Parts Network

In this paper, we present a new method, called Pose-over-Parts Network (PoP-Net), for multi-person 3D pose estimation from depth images. Our method first uses an efficient one-shot network to predict part-level representations and global poses, and then fuses the positional-precise part detection and structurally valid global poses in an explicit way.

The pipeline of PoP-Net is composed of a backbone network, a global pose network, and three functional branches: heatmap branch, depth branch, and TPDF branch, as illustrated in Figure 3. The two-stage split-and-merge design is inspired by OpenPose [Cao *et al.*, 2017] and mostly follows the simplified version applied to depth input [Martínez-González *et al.*, 2018]. PoP-Net outputs three sets of part maps from the second stage of functional branches and an anchor-based global pose map from the global pose network.

Supposing each human body includes  $K$  body parts, the heatmap branch outputs a set of part confidence maps  $\{H_j\}_{j=1}^{K+1}$ , where each  $H_j$  describes the confidence of a body part occurring at each discrete location in the first  $K$  maps, and the last map describes the background confidence. The depth branch outputs a set of maps  $\{D_j\}_{j=1}^K$ , where each  $D_j$  encodes the depth map associated with part  $j$ .

The core of our method is a new part-level representation, called Truncated Part Displacement Field (TPDF). For each part type  $j$ , TPDF records a displacement vector pointing to the *closest* part instance for every 2D position. The uniqueness of the proposed TPDF is two fold: (1) it encodes the displacement field involving multiple parts of the same type in a single map, and (2) it is only effective in a *truncated* range which enables the learning of convolutional kernels. The TPDF branch outputs TPDFs represented as a set of  $x$ -axis displacement maps  $\{X_j\}_{j=1}^K$  and a set of  $y$ -axis displacement maps  $\{Y_j\}_{j=1}^K$ .

Compared to previous methods which predict person-wise part displacements [Papandreou *et al.*, 2017; Xiong *et al.*, 2019], TPDF processes at image level and is able to handle multiple bodies in one pass. While compared to the Part Affinity Field introduced in OpenPose [Cao *et al.*, 2017], TPDF not only saves the heavy bipartite matching process, but also enables a simple fusion process to take advantage of both global and local predictions, which increases robustness in handling truncation, occlusion and multi-person conflict.

At last, a global pose map  $P$  is regressed from the global

pose network. As shown in Figure 6, the global pose network is a direct extension from Yolo2 [Redmon and Farhadi, 2017], where both bounding box attributes and additional 3D pose attributes are regressed with respect to the anchors associated with each grid. A set of predicted global poses are then extracted via conducting an NMS on the global pose map  $P$ .

### Training

PoP-Net is trained end-to-end via minimizing the total loss  $\mathcal{L}$  which is the sum of heatmap loss  $\mathcal{L}_h$ , depth loss  $\mathcal{L}_d$ , TPDF loss  $\mathcal{L}_t$ , and global pose loss  $\mathcal{L}_p$ . As shown in Figure 3, losses corresponding to the functional branches are contributed from multiple stages of the network. Specifically, the loss function can be written as:

$$\mathcal{L} = \mathcal{L}_h + \mathcal{L}_d + \mathcal{L}_t + \mathcal{L}_p \quad (1)$$

$$\mathcal{L}_h = \sum_{s=1}^S \sum_{j=1}^{K+1} \|H_j^s - H_j^*\|_2^2 \quad (2)$$

$$\mathcal{L}_d = \sum_{s=1}^S \sum_{j=1}^K W_j^d \cdot \|D_j^s - D_j^*\|_2^2 \quad (3)$$

$$\mathcal{L}_t = \sum_{s=1}^S \sum_{j=1}^K W_j^t \cdot (\|X_j^s - X_j^*\|_2^2 + \|Y_j^s - Y_j^*\|_2^2) \quad (4)$$

$$\mathcal{L}_p = W^p \cdot \|P - P^*\|_2^2 \quad (5)$$

where  $s$  indicates the stage of the network, and uses  $S = 2$  stages. More specifically,  $H_j^*$ ,  $D_j^*$ ,  $X_j^*$ ,  $Y_j^*$ , and  $P^*$  indicate the ground-truth maps while  $W_j^d$ ,  $W_j^t$ , and  $W^p$  indicate the point-wise weight maps in the same dimension as the corresponding ground-truth maps. Weight maps are not applied to heatmap loss as the foreground and background samples are treated equally important. The details of the preparation of ground-truth map and weight map are illustrated later together with the architecture for each network component.

### Fusion process

TPDF enables a post-process to fuse part representations and global poses. As illustrated in Figure 1, a 2D part predicted from a global pose located at  $(x_j, y_j)$  is dragged to an updated position  $(\hat{x}_j, \hat{y}_j)$  following the displacement vector predicted in the TPDF of part  $j$ , such that  $\hat{x}_j = x_j + X_j(x_j, y_j)$ ,  $\hat{y}_j = y_j + Y_j(x_j, y_j)$ . To improve accuracy, weighted aggregation is applied to estimate the final 2D position  $\{(\hat{x}_j, \hat{y}_j)\}_{j=1}^K$  and

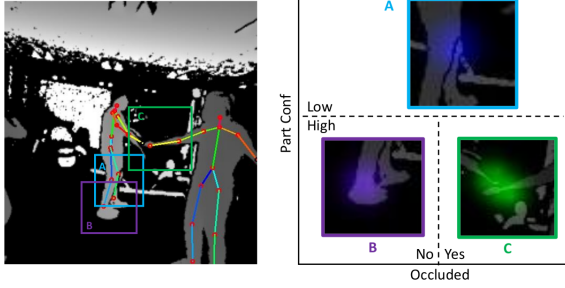


Figure 4: **Conflicting cases to resolve in fusion.** Part confidence maps for the marked regions are visualized to illustrate three conflicting cases to resolve. A: The confidence of left knee is low. B: The confidence of right foot is high without ambiguity. C: The confidence of occluded right hand is high but hallucinated by the same part from another person.

depth  $\{\hat{Z}_j\}_{j=1}^K$ , as illustrated in Figure 1. Specifically,  $X_j$ ,  $Y_j$ , and  $D_j$  within a mask  $M$  centered at the updated integer position  $(\lfloor \hat{x}_j \rfloor, \lfloor \hat{y}_j \rfloor)$  is averaged by using  $H_j$  as aggregation weights, which leads to the following equations:

$$\hat{x}_j = \lfloor \hat{x}_j \rfloor + \frac{\sum_{(u,v) \in M} H_j(u,v) \cdot X_j(u,v)}{\sum_{(u,v) \in M} H_j(u,v)} \quad (6)$$

$$\hat{y}_j = \lfloor \hat{y}_j \rfloor + \frac{\sum_{(u,v) \in M} H_j(u,v) \cdot Y_j(u,v)}{\sum_{(u,v) \in M} H_j(u,v)} \quad (7)$$

$$\hat{Z}_j = \frac{\sum_{(u,v) \in M} H_j(u,v) \cdot D_j(u,v)}{\sum_{(u,v) \in M} H_j(u,v)}. \quad (8)$$

Predicted  $\{(\hat{x}_j, \hat{y}_j)\}_{j=1}^K$  and  $\{\hat{Z}_j\}_{j=1}^K$  are transformed to 3D positions given known camera intrinsic parameters.

### Resolving conflicting cases

There are conflicting cases when multiple human bodies occlude each other or a global pose falls out of the effective range of a TPDF. To resolve the conflicting cases, a mode selection scheme is carefully designed that is based on the part confidence maps  $\{H_j\}_{j=1}^{K+1}$  from the heatmap branch and the part visibility attributes from the global pose network.

As illustrated in Figure 4, there are in total three cases to consider respectively: (A) when the part confidence  $H_j$  is low at a global part position, the global detection is used directly, which is usually observed when the position of a part is not accessible due to truncation or occlusion; (B) when the part confidence is high and no occlusion from another instance of the same part is involved, the presented fusion process is applied; and (C) a challenging case may occur when the part confidence is high but is impacted by occlusion from another instance of the same part type. Fortunately, this case can be detected by introducing additional part visibility  $\{v_j\}_{j=1}^K$  to the global pose representation. Since the part depth map is prepared following a  $z$ -buffer rule, a significant difference between the global part depth and the part depth map will be observed in this case.

## 2.1 Regression networks

The network architecture and ground truth preparation for each component will be described in detail.

### Backbone network

The backbone network is implemented to include layers 0-2 from ResNet-34 [He *et al.*, 2016] for general image encoding. It outputs a  $\frac{w}{8} \times \frac{h}{8} \times 128$  feature map, where  $h$  and  $w$  indicate height and width of an input image respectively. We choose to maintain  $8 \times$  downsampling level in the following functional branches to make part-level inference both efficient and capable of handling human parts at a distance.

### Heatmap branch

The heatmap branch is designed to predict  $K + 1$  confidence maps corresponding to  $K$  body part and the background. The heatmap branch is made of five  $3 \times 3$  convolutional layers as illustrated in Figure 5 (a). It is worth noting that every convolutional layer mentioned in our method is followed by BN and ReLU layers. To prepare ground-truth part confidence maps  $\{H_j^*\}_{j=1}^{K+1}$ , we adopt the same method introduced in OpenPose [Cao *et al.*, 2017], which applies a Gaussian filter at each part location.

### Depth branch

The depth branch predicts part-wise depth maps, which is meaningful in relieving the effect from raw depth artifacts and in recovering the true depth of a part under occlusion. The network is made of five convolutional layers whose specific architecture is shown in Figure 5 (b).

To prepare ground-truth depth maps  $\{D_j^*\}_{j=1}^K$ , each map is initialized with the resized raw depth input. The depth values within a 2-pixel-radius disk centered at each part  $j$  are overridden with the ground-truth depth of part  $j$ , as illustrated in Figure 5 (b). In a multi-person scenario, if a 2D grid position is occupied by masks of more than one part instance, the writing of depth values follows a standard  $z$ -buffer rule where the smallest depth value is recorded. In addition, the weight maps  $\{W_j^d\}_{j=1}^K$  are prepared in the same dimension as the ground-truth depth maps. We use weight 0.9 for a foreground grid while 0.1 for the background.

### TPDF branch

TPDF maps are predicted from the TPDF branch implemented following the architecture as shown in Figure 5 (c). During ground-truth preparation,  $\{X_j^*\}_{j=1}^K$  and  $\{Y_j^*\}_{j=1}^K$  are prepared so that the displacement vector at a 2D position points to the closest part position. Specifically, the displacement vector is only non-zero within the truncated range ( $r = 2$ ) from each part position, as shown in Figure 5 (c). The preparation of weight maps  $\{W_j^t\}_{j=1}^K$  is similar to the process for the depth branch. However, the weights within the truncated mask is set to 1.0 and the rest is set to strict 0. Adopting truncated range is critical for training convolutional kernels. If a full-range field is used, a pair of displacement vectors close to each other but far from any part may have huge difference in  $X, Y$  values. In such cases, the training of convolutional kernels will be confused by image patches similar in appearance but associated with different values.

### Global pose network

The global pose network predicts a global pose map from concatenated features from the backbone and functional branches. The network includes four convolutional layers



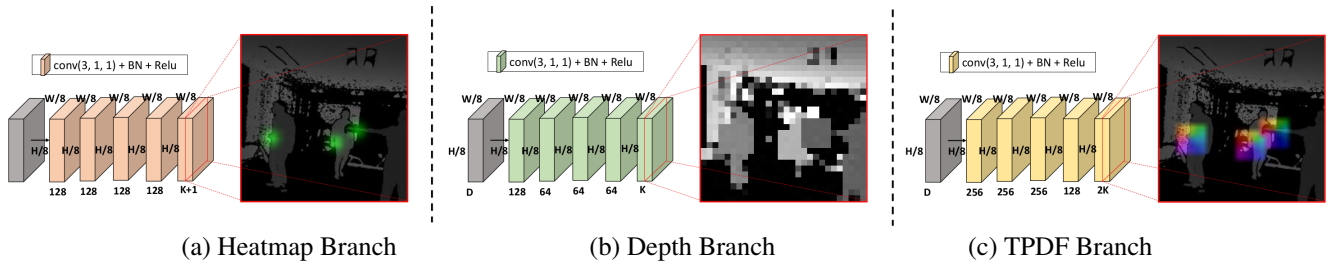


Figure 5: **Functional branches.** (a) The heatmap branch predicts  $K$  confidence maps for body parts with an additional map for background. (b) The depth branch outputs  $K$  depth maps for  $K$  body parts, respectively. (c) The TPDF branch outputs  $2K$  maps of displacement vectors  $\{X_j\}_{j=1}^K, \{Y_j\}_{j=1}^K$ . The field visualization follows the optical flow standard.

where the first is followed by a max pooling to cast the feature map to  $16\times$  downsampling level, as shown in Figure 6.

The ground-truth preparation process is similar to Yolo2 [Redmon and Farhadi, 2017]. Specifically, the ground-truth global pose map  $P^*$  is prepared so that each grid records five bounding box attributes and a set of pose attributes  $\{(dx_j^a, dy_j^a, Z_j^a, v_j^a)\}_{j=1}^K$  of the ground-truth pose for each associated anchor  $a$ . Specifically,  $(dx_j^a, dy_j^a)$  indicate the 2D offsets of part  $j$  from the anchor center,  $Z_j^a$  indicates the 3D part depth, and  $v_j^a$  indicates the visibility of part  $j$ . The value of  $v_j^a$  is assigned to 1 when the depth from a global pose part  $Z_j^a$  is different from the corresponding depth branch ground-truth in  $D_j$ , otherwise it is assigned to 0. The weight map  $W^p$  is prepared in the same dimension as  $P^*$ . For the dimensions corresponding to bounding box probabilities, 0.9 is applied to the grids associated with ground truth, while 0.1 is assigned to the rest. For the other dimensions, the weights are strictly assigned to 1 or 0. The weight map is designed in such way because the detection task related to  $p_b$  considers both foreground and background while the regression task to other attributes focuses on foreground.

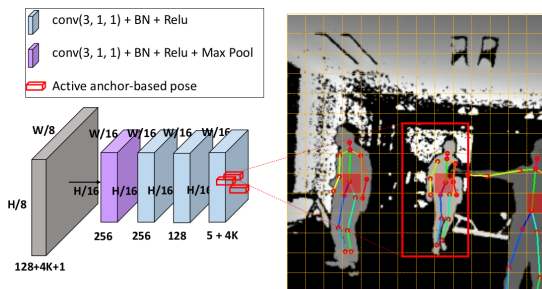


Figure 6: **Global pose network.** The global pose network is composed of four  $3 \times 3$  convolutional layers, where an additional max-pooling is involved in the first layer. The network outputs an anchor-based global pose map, which is converted to a set of poses after NMS.

### 3 KD3DH: Kinect Depth 3D Human Dataset

Due to the lack of high-quality depth datasets for 3D pose estimation, we propose the Kinect Depth 3D Human Dataset (KD3DH) to boost the development and evaluation of 3D pose estimation targeting real-world multi-person challenges.

There are a few existing depth datasets for human pose estimation, but the data quality and diversity is rather limited. DIH [Martínez-González *et al.*, 2018] and K2HPD [Wang *et al.*, 2016] include a decent amount of data but are limited to 2D poses. ITOP [Haque *et al.*, 2016] is a widely tested depth dataset for 3D pose estimation. However, data from ITOP is strictly limited to single person, clean background, and low diversity in object scales, camera angles, and pose types.

KD3DH was constructed to ensure data sufficiency and diversity in human poses, object scales, camera angles, truncation scenarios, background scenes, and dynamic occlusions. In practice, collecting enough data to represent multi-person configurations combined with different background scenes is an intractable task due to combinatorial explosion. To maintain the cost, we only cover the diversity types not achievable with data composition or data augmentation. Specifically, in KD3DH, real data collection focuses on single person data involving varying poses, different object scales, varying camera ray angles, and additional pure background data covering different types of scenes. The remaining types of diversity are ensured via data composition and data augmentation given the fact that foreground masks of the recorded human instances are available.

Set	Img	Sbj	Loc	Ori	Act	Sn	L+
train	176828	13	4+	4	10+	1	seg
val	32719	2	4+	4	10+	1	seg
bg	8680	0	0	0	0	8	no
test	4484	5	0	0	free	4	mp

Table 1: **KD3DH Summary.** The total number of images (Img), human subjects (Sbj), recording locations (Loc), self-orientations (Ori), action types (Act), scenes (Sn) are summarized. Additional label type (L+) indicates whether a set has segmentation (seg) or multi-person (mp) labels.

#### Construction procedure

We utilize Azure Kinect to record human depth videos and automatically extract 3D human poses associated with each depth image. Overall, 20 human candidates were involved in the recording procedure; 15 of them were recorded individually to construct the training set, while the remaining five were recorded in multi-person sessions to produce the multi-person test set. For the training set, each candidate was

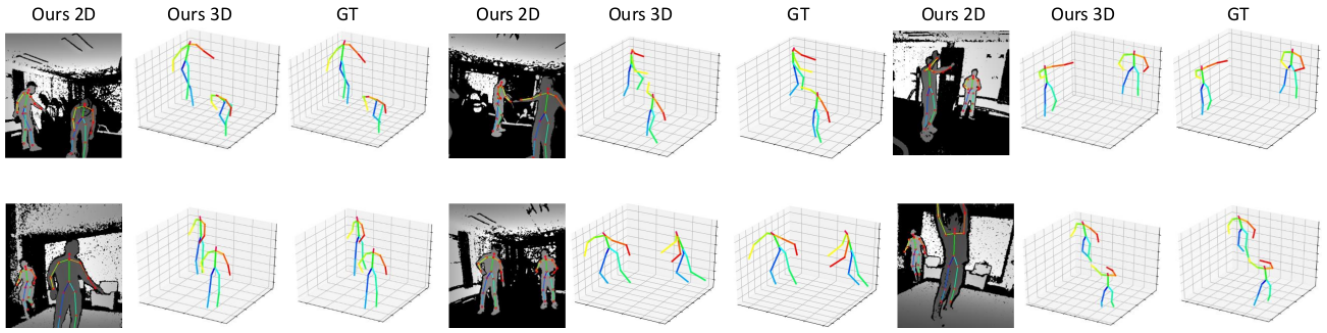


Figure 7: **PoP-Net Visual Results.** Predictions in 2D, 3D, and the ground-truth are visualized on six examples from KD3DH.

recorded with a clean background in four trials at four different locations within the camera frustum. In each trial, a candidate was asked to repeat 10 predetermined actions while facing four different orientations spanning  $360^\circ$  and an additional short sequence of free-style movements towards the end. A classic graph-cut based method was applied to produce human segments for the training set. In addition, background images were recorded separately with moderate camera movements from eight different scenes. For the testing set, the remaining five people were recorded while performing random actions with different combinations in four different scenes. Human annotations have been conducted both in the training and testing sets to sift out the erroneous 3D poses generated from Kinect. An interactive verification tool was developed to remove unqualified samples from the raw collection. Table 1 shows the statistics of our KD3DH dataset.

## 4 Experiments

### Datasets

We evaluate our method on two benchmarks for 3D pose estimation methods given a depth image as input: the KD3DH dataset and ITOP [Haque *et al.*, 2016] dataset. KD3DH includes highly diverse 3D human data across different visual aspects and provides reliable human segments to enable background augmentation and multi-person augmentation. The evaluation on KD3DH aims to determine a method’s capability in handling the real-world challenges of multi-person 3D pose estimation. Meanwhile, ITOP is a widely tested dataset for single-person 3D pose under highly controlled environment. We report results on ITOP to compare with prior state-of-the-arts on a simplified task.

### Evaluation metric

We apply both mAP and PCK metrics to evaluate a method from different aspects. First, PCK is a measurement that focuses on pose estimation without considering redundant detections. In our experiments, PCK is calculated as the average percentage of accurate key points on the best-matched predictions to the ground-truth poses, where the best match is based on the IOU of 2D bounding boxes. We use the method introduced in MPII [Andriluka *et al.*, 2014] dataset with 2D and 3D threshold set the same way compared to PCK. Second, mAP is an overall metric considering both object detection and pose estimation accuracy. For both PCK and mAP, 0.5-

head size rule is applied for 2D while 10-cm rule is applied for 3D.

### Competing methods

A few prototypical methods have been compared with our method: (a) Yolo-Pose+ represents a typical top-down method, which is a pose estimation network extended from yolo-v2 [Redmon and Farhadi, 2017] and implemented by us; (b) Open-Pose+ is a pure bottom-up method that is an extension from RPM [Martínez-González *et al.*, 2018], a simplified version of OpenPose [Cao *et al.*, 2017]) that we extended with an additional depth branch so that it detects multiple 3D poses from depth input; and (c) A2J [Xiong *et al.*, 2019] represents the state-of-the-art two-stage pose estimation given a depth image as input.

To conduct a fair comparison of candidate methods, Yolo-Pose+, Open-Pose+, and PoP-Net are implemented using as many identical modules as possible. Specifically, Yolo-Pose+ is composed of the backbone network, the global pose network proposed for PoP-Net, and five additional intermediate  $3 \times 3$  convolutional layers with  $256d$  features in between. Open-Pose+ integrates the same backbone network, the heatmap branch, the depth branch from PoP-Net, and an additional Part Affinity Field (PAF) branch proposed in [Cao *et al.*, 2017]. The pose-process of Open-Pose+ follows the original work to use bipartite matching upon PAF to assemble detected parts into human bodies, and in addition reads the depth branch output to produce 3D poses. For A2J [Xiong *et al.*, 2019], we use the identical network presented in the original paper for simplicity. Because A2J needs to work with given bounding-boxes for the multi-person case, we provide it with the predicted bounding boxes from Yolo-Pose+ such that the bounding-box quality is comparable to the other methods.

### Implementation details

The input depth images are resized to  $224 \times 224$  for Yolo-Pose+, Open-Pose+, and PoP-Net. The images are cropped and resized to  $288 \times 288$  for A2J. Yolo-Pose+, Open-Pose+, PoP-Net are trained via standard SGD optimizer for 100 epochs, while A2J is trained via Adam optimizer following the original paper. Yolo-Pose+, Open-Pose+, PoP-Net use two anchors with size  $6 \times 12$ , and  $3 \times 6$ , respectively. An identical data augmentation process is applied to every method, and the basic data augmentation process applied to both KD3DH and ITOP includes random rotation, flipping,

cropping, and a specific depth augmentation detailed in Appendix A.

#### 4.1 KD3DH dataset

On the KD3DH dataset, a method is trained on the training set which not only provides 3D human poses but also human segments. Given the provided human segments, background augmentation can be applied by superimposing the human mask region from a training image onto a randomly selected background image. Meanwhile, multi-person augmentation can also be applied by superimposing multiple human segments onto a random background scene following  $z$ -buffer rule. In training, each method is trained with multi-person augmentation on top of basic data augmentation. The multi-person augmentation is described in detail in Appendix B.

In testing, a method is evaluated on four different datasets representing different levels of challenges: (1) the validation set directly (**simple**), (2) the background augmented set constructed from validation set (**bg aug**), (3) the multi-person augmented set constructed from validation set (**mp aug**), and (4) the real testing set including challenging real-world, multi-person recordings (**mp real**). Visual results of PoP-Net on the last set are shown in Figure 7. More qualitative comparisons on challenging cases are provided in Appendix D.

#### Ablation study

We conducted an ablation study for PoP-Net to differentiate the contribution from different components. As shown in Table 2, evaluation has been done separately on: (1) the 2D global poses predicted from the global pose network (**2D Glb**), (2) the final 2D poses after fusion (**2D Fuse**), (3) the 3D global poses predicted from the global pose network (**3D Glb**), (4) the 3D poses computed from 2D fused poses and predicted depth of parts (**3D Fuse**), and (5) the upper bound of 3D poses computed from ground-truth 2D poses and predicted depth (**3D UB**). As observed, 2D/3D poses after fusion constantly improve the direct outputs from the global pose network, and the margin increases on more challenging testing set. It can also be observed that the accuracy of 3D poses drops more significantly compared to 2D on more challenging datasets, where the upper bound is still far from ideal. This indicates that future work has huge room to improve on depth prediction under multi-person occlusion.

Metric	Test	2D Glb	2D Fuse	3D Glb	3D Fuse	3D UB
mAP	simple	0.963	0.974	0.917	0.926	0.931
	bg aug	0.965	0.977	0.915	0.924	0.927
	mp aug	0.849	0.863	0.701	0.708	0.735
	mp real	0.755	0.799	0.582	0.606	0.622
PCK	simple	0.968	0.978	0.939	0.947	0.956
	bg aug	0.970	0.982	0.938	0.947	0.953
	mp aug	0.898	0.906	0.794	0.808	0.846
	mp real	0.798	0.839	0.681	0.708	0.756

Table 2: **Ablation study of PoP-Net.** 2D global pose (2D Glb), 2D fused output (2D Fuse), 3D global pose (3D Glb), 3D fused output (3D Fuse) and 3D pose upper unbound (3D UB) are reported on four testing sets, in mAP and PCK, respectively.

#### Quantitative comparison

PoP-Net is compared to other methods on KD3DH on four different testing sets. As observed in Table 3, overall PoP-Net achieves the STOA under every testing set, which significantly surpasses other methods under the most challenging metric, 3D mAP on mp real test. Open-Pose+ is observed to have marginal advantages in 2D mAP for certain tests because it gains higher recall via detecting parts without seeing the whole body. However the pure bottom-up decision leads to erroneous depth prediction under occlusion, such that its 3D mAP drops significantly. A2J, on the other hand, shows marginal advantage in 3D PCK for certain tests. This can be interpreted that the global weighted aggregation in A2J can leverage the full context information from the ROI to predict part depth under occlusion. However, A2J appears to be rather sensitive to the predicted ROIs such that its mAP performance is not optimal.

Test	Method	2D PCK	3D PCK	2D mAP	3D mAP
simple	Yolo-Pose+	0.957	0.910	0.926	0.847
	Open-Pose+	<b>0.967</b>	0.915	<b>0.967</b>	<b>0.893</b>
	Yolo-A2J	0.959	<b>0.924</b>	0.936	0.868
	PoP-Net	<b>0.978</b>	<b>0.947</b>	<b>0.974</b>	<b>0.926</b>
bg aug	Yolo-Pose+	0.956	0.904	0.923	0.834
	Open-Pose+	0.911	0.916	<b>0.969</b>	<b>0.885</b>
	Yolo-A2J	<b>0.964</b>	<b>0.927</b>	0.941	0.871
	PoP-Net	<b>0.982</b>	<b>0.947</b>	<b>0.977</b>	<b>0.924</b>
mp aug	Yolo-Pose+	0.872	0.777	0.799	0.651
	Open-Pose+	<b>0.887</b>	0.765	<b>0.870</b>	0.667
	Yolo-A2J	0.876	<b>0.819</b>	0.803	<b>0.707</b>
	PoP-Net	<b>0.906</b>	<b>0.808</b>	<b>0.863</b>	<b>0.708</b>
mp real	Yolo-Pose+	0.734	0.607	0.616	0.449
	Open-Pose+	0.805	0.641	<b>0.802</b>	0.558
	Yolo-A2J	<b>0.837</b>	<b>0.724</b>	0.744	<b>0.574</b>
	PoP-Net	<b>0.839</b>	<b>0.708</b>	<b>0.799</b>	<b>0.606</b>

Table 3: **Evaluation on KD3DH dataset.** Competing methods are evaluated on four different testing sets. For each test set, the best method is marked in bold black while the second best method is marked in blue.

#### 4.2 ITOP dataset

PoP-Net is compared with competing methods on the ITOP dataset. Because ITOP is limited to single-person and clean background, it is not perfect for evaluating PoP-Net which is designed for multi-person tasks. Meanwhile, PCK and mAP measurements are mostly identical, therefore we only report 2D PCK metrics on ITOP. To conduct a fair comparison, a method is trained and tested under two setups separately. One is based on provided ground-truth bounding boxes and the other directly uses the full image, as shown in Table 4. It can be observed that PoP-Net consistently outperforms Open-Pose+ and Yolo-Pose+ by a significant margin. Compared to A2J, PoP-Net is slightly worse in 3D and better in 2D. This is consistent with the PCK results reported on KD3DH dataset.

#### 4.3 Running speed analysis

The efficiency of all the methods are compared on multi-person test (2-3 people) measured in FPS. The calculation of



Exp Setup	Method	2D PCK	3D PCK
GT Bbox	A2J	0.905	<b>0.891</b>
	PoP-Net	<b>0.914</b>	0.882
Full Image	Yolo-Pose+	0.833	0.787
	Open-Pose+	0.876	0.778
	Yolo-A2J	0.873	<b>0.854</b>
	PoP-Net	<b>0.890</b>	<b>0.843</b>

Table 4: **Evaluation on ITOP (front-view)**. Methods are evaluated on ITOP dataset with and without GT Bbox.

running speed considers necessary post-processing to achieve the final set of multiple 3D poses and the bounding box prediction time for a two-stage method. As shown in Table 5, the running speed of PoP-Net almost triples A2J and doubles Open-Pose+ on a single RTX 2080Ti GPU. The observation is as expected because OpenPose+ involves heavier post process and A2J’s cost scales up with the number of humans. More detailed analysis is provided in Appendix C.

	Yolo-Pose+	Open-Pose+	A2J	PoP-Net
FPS	223	48	32	91

Table 5: **Running speed on multi-person data.**

## 5 Conclusion

In this paper, we introduce PoP-Net for multi-person 3D pose estimation from a depth image. Our methods predicts part maps and global poses in a single shot and explicitly fuse them via leveraging the proposed Truncated Part Displacement Field (TPDF). Conflicting cases are effortlessly resolved in a rule-based process taking part visibility and confidence output from PoP-Net. A comprehensive 3D human depth dataset, called KD3DH, is released to facilitate the development of models for real-world multi-person challenges. In experiments, PoP-Net achieves state-of-the-art results on both KD3DH and ITOP dataset with significant improvements in running speed in processing multi-person data.

### Acknowledgements

This work was supported by OPPO US Research Center.

### References

[Andriluka *et al.*, 2014] Mykhaylo Andriluka, Leonid Pishchulin, Peter V. Gehler, and Bernt Schiele. 2d human pose estimation: New benchmark and state of the art analysis. In *IEEE Conference on Computer Vision and Pattern Recognition (CVPR)*, pages 3686–3693, 2014.

[Cao *et al.*, 2017] Zhe Cao, Tomas Simon, Shih-En Wei, and Yaser Sheikh. Realtime multi-person 2d pose estimation using part affinity fields. In *IEEE Conference on Computer Vision and Pattern Recognition (CVPR)*, pages 1302–1310, 2017.

[Elhayek *et al.*, 2017] Ahmed Elhayek, Edilson de Aguiar, Arjun Jain, Jonathan Tompson, Leonid Pishchulin,

Mykhaylo Andriluka, Christoph Bregler, Bernt Schiele, and Christian Theobalt. Marconi - convnet-based markerless motion capture in outdoor and indoor scenes. *IEEE Trans. Pattern Anal. Mach. Intell.*, 39(3):501–514, 2017.

[Fang *et al.*, 2017] Haoshu Fang, Shuqin Xie, Yu-Wing Tai, and Cewu Lu. RMPE: regional multi-person pose estimation. In *IEEE International Conference on Computer Vision (ICCV)*, pages 2353–2362, 2017.

[Haque *et al.*, 2016] Albert Haque, Boya Peng, Zelun Luo, Alexandre Alahi, Serena Yeung, and Fei-Fei Li. Towards viewpoint invariant 3d human pose estimation. In *14th European Conference Computer Vision (ECCV)*, pages 160–177, 2016.

[He *et al.*, 2016] Kaiming He, Xiangyu Zhang, Shaoqing Ren, and Jian Sun. Deep residual learning for image recognition. In *IEEE Conference on Computer Vision and Pattern Recognition (CVPR)*, pages 770–778, 2016.

[He *et al.*, 2017] Kaiming He, Georgia Gkioxari, Piotr Dollár, and Ross B. Girshick. Mask R-CNN. In *IEEE International Conference on Computer Vision (ICCV)*, pages 2980–2988, 2017.

[Ionescu *et al.*, 2014] Catalin Ionescu, Dragos Papava, Vlad Olaru, and Cristian Sminchisescu. Human3.6m: Large scale datasets and predictive methods for 3d human sensing in natural environments. *IEEE Trans. Pattern Anal. Mach. Intell.*, 36(7):1325–1339, 2014.

[Iqbal and Gall, 2016] Umar Iqbal and Juergen Gall. Multi-person pose estimation with local joint-to-person associations. In *European Conference on Computer Vision Workshops*, pages 627–642, 2016.

[Kanazawa *et al.*, 2018] Angjoo Kanazawa, Michael J. Black, David W. Jacobs, and Jitendra Malik. End-to-end recovery of human shape and pose. In *IEEE Conference on Computer Vision and Pattern Recognition (CVPR)*, pages 7122–7131, 2018.

[Lin *et al.*, 2014] Tsung-Yi Lin, Michael Maire, Serge J. Belongie, James Hays, Pietro Perona, Deva Ramanan, Piotr Dollár, and C. Lawrence Zitnick. Microsoft COCO: common objects in context. In *13th European Conference on Computer Vision (ECCV)*, pages 740–755, 2014.

[Liu *et al.*, 2016] Wei Liu, Dragomir Anguelov, Dumitru Erhan, Christian Szegedy, Scott E. Reed, Cheng-Yang Fu, and Alexander C. Berg. SSD: single shot multibox detector. In *14th European Conference on Computer Vision (ECCV)*, pages 21–37, 2016.

[Martinez *et al.*, 2017] Julieta Martinez, Rayat Hossain, Javier Romero, and James J. Little. A simple yet effective baseline for 3d human pose estimation. In *IEEE International Conference on Computer Vision (ICCV)*, pages 2659–2668, 2017.

[Martínez-González *et al.*, 2018] Ángel Martínez-González, Michael Villamizar, Olivier Canévet, and Jean-Marc Odobez. Real-time convolutional networks for depth-based human pose estimation. In *IEEE/RSJ International Conference on Intelligent Robots and Systems (IROS)*, pages 41–47, 2018.



- [Mehta *et al.*, 2017] Dushyant Mehta, Srinath Sridhar, Oleksandr Sotnychenko, Helge Rhodin, Mohammad Shafiei, Hans-Peter Seidel, Weipeng Xu, Dan Casas, and Christian Theobalt. Vnect: real-time 3d human pose estimation with a single RGB camera. *ACM Trans. Graph.*, 36(4):44:1–44:14, 2017.
- [Mehta *et al.*, 2018] Dushyant Mehta, Oleksandr Sotnychenko, Franziska Mueller, Weipeng Xu, Srinath Sridhar, Gerard Pons-Moll, and Christian Theobalt. Single-shot multi-person 3d pose estimation from monocular RGB. In *International Conference on 3D Vision (3DV)*, pages 120–130, 2018.
- [Mehta *et al.*, 2019] Dushyant Mehta, Oleksandr Sotnychenko, Franziska Mueller, Weipeng Xu, Mohamed Elgharib, Pascal Fua, Hans-Peter Seidel, Helge Rhodin, Gerard Pons-Moll, and Christian Theobalt. Xnect: Real-time multi-person 3d human pose estimation with a single RGB camera. *CoRR*, abs/1907.00837, 2019.
- [Newell *et al.*, 2016] Alejandro Newell, Kaiyu Yang, and Jia Deng. Stacked hourglass networks for human pose estimation. In Bastian Leibe, Jiri Matas, Nicu Sebe, and Max Welling, editors, *14th European Conference on Computer Vision (ECCV)*, pages 483–499, 2016.
- [Newell *et al.*, 2017] Alejandro Newell, Zhiao Huang, and Jia Deng. Associative embedding: End-to-end learning for joint detection and grouping. In Isabelle Guyon, Ulrike von Luxburg, Samy Bengio, Hanna M. Wallach, Rob Fergus, S. V. N. Vishwanathan, and Roman Garnett, editors, *Annual Conference on Neural Information Processing Systems*, pages 2277–2287, 2017.
- [Omran *et al.*, 2018] Mohamed Omran, Christoph Lassner, Gerard Pons-Moll, Peter V. Gehler, and Bernt Schiele. Neural body fitting: Unifying deep learning and model based human pose and shape estimation. In *International Conference on 3D Vision (3DV)*, pages 484–494, 2018.
- [Papandreou *et al.*, 2017] George Papandreou, Tyler Zhu, Nori Kanazawa, Alexander Toshev, Jonathan Tompson, Chris Bregler, and Kevin Murphy. Towards accurate multi-person pose estimation in the wild. In *IEEE Conference on Computer Vision and Pattern Recognition (CVPR)*, 2017.
- [Pavlakos *et al.*, 2017] Georgios Pavlakos, Xiaowei Zhou, Konstantinos G. Derpanis, and Kostas Daniilidis. Coarse-to-fine volumetric prediction for single-image 3d human pose. In *IEEE Conference on Computer Vision and Pattern Recognition (CVPR)*, pages 1263–1272, 2017.
- [Pavlakos *et al.*, 2018] Georgios Pavlakos, Xiaowei Zhou, and Kostas Daniilidis. Ordinal depth supervision for 3d human pose estimation. In *IEEE Conference on Computer Vision and Pattern Recognition (CVPR)*, pages 7307–7316, 2018.
- [Pishchulin *et al.*, 2016] Leonid Pishchulin, Eldar Insafutdinov, Siyu Tang, Bjoern Andres, Mykhaylo Andriluka, Peter V. Gehler, and Bernt Schiele. Deepcut: Joint subset partition and labeling for multi person pose estimation. In *IEEE Conference on Computer Vision and Pattern Recognition (CVPR)*, pages 4929–4937, 2016.
- [Redmon and Farhadi, 2017] Joseph Redmon and Ali Farhadi. YOLO9000: better, faster, stronger. In *IEEE Conference on Computer Vision and Pattern Recognition (CVPR)*, pages 6517–6525, 2017.
- [Redmon *et al.*, 2016] Joseph Redmon, Santosh Kumar Divvala, Ross B. Girshick, and Ali Farhadi. You only look once: Unified, real-time object detection. In *IEEE Conference on Computer Vision and Pattern Recognition (CVPR)*, pages 779–788, 2016.
- [Ren *et al.*, 2017] Shaoqing Ren, Kaiming He, Ross B. Girshick, and Jian Sun. Faster R-CNN: towards real-time object detection with region proposal networks. *IEEE Trans. Pattern Anal. Mach. Intell.*, 39(6):1137–1149, 2017.
- [Rhodin *et al.*, 2016] Helge Rhodin, Nadia Robertini, Dan Casas, Christian Richardt, Hans-Peter Seidel, and Christian Theobalt. General automatic human shape and motion capture using volumetric contour cues. In *14th European Conference on Computer Vision (ECCV)*, pages 509–526, 2016.
- [Rogez *et al.*, 2020] Grégory Rogez, Philippe Weinzaepfel, and Cordelia Schmid. Lcr-net++: Multi-person 2d and 3d pose detection in natural images. *IEEE Trans. Pattern Anal. Mach. Intell.*, 42(5):1146–1161, 2020.
- [Tekin *et al.*, 2016] Bugra Tekin, Isinsu Katircioglu, Mathieu Salzmann, Vincent Lepetit, and Pascal Fua. Structured prediction of 3d human pose with deep neural networks. In *British Machine Vision Conference (BMVC)*, 2016.
- [Wang *et al.*, 2016] Keze Wang, Shengfu Zhai, Hui Cheng, Xiaodan Liang, and Liang Lin. Human pose estimation from depth images via inference embedded multi-task learning. In *ACM Conference on Multimedia Conference*, pages 1227–1236, 2016.
- [Wei *et al.*, 2016] Shih-En Wei, Varun Ramakrishna, Takeo Kanade, and Yaser Sheikh. Convolutional pose machines. In *IEEE Conference on Computer Vision and Pattern Recognition (CVPR)*, pages 4724–4732, 2016.
- [Xiong *et al.*, 2019] Fu Xiong, Boshen Zhang, Yang Xiao, Zhiguo Cao, Taidong Yu, Joey Tianyi Zhou, and Junsong Yuan. A2J: anchor-to-joint regression network for 3d articulated pose estimation from a single depth image. In *IEEE/CVF International Conference on Computer Vision (ICCV)*, pages 793–802, 2019.
- [Zanfir *et al.*, 2018] Andrei Zanfir, Elisabeta Marinoiu, Mihai Zanfir, Alin-Ionut Popa, and Cristian Sminchisescu. Deep network for the integrated 3d sensing of multiple people in natural images. In Samy Bengio, Hanna M. Wallach, Hugo Larochelle, Kristen Grauman, Nicolò Cesa-Bianchi, and Roman Garnett, editors, *Advances in Neural Information Processing Systems*, pages 8420–8429, 2018.
- [Zhou *et al.*, 2017] Xingyi Zhou, Qixing Huang, Xiao Sun, Xiangyang Xue, and Yichen Wei. Towards 3d human pose estimation in the wild: A weakly-supervised approach. In *IEEE International Conference on Computer Vision (ICCV)*, pages 398–407, 2017.

## A Depth Augmentation

Given camera intrinsic parameters and the measured depth, new depth maps and their associated 2D/3D pose labels can be simulated via simulating the camera is moved to another location along the principle axis to capture the depth data. Specifically, in this case, a 3D point  $(X, Y, Z_0)$  in the original camera coordinate frame with projection at  $(x_0, y_0)$  in the original image will be located at  $(X, Y, Z_1)$  in the new camera coordinate frame and be projected to  $(x_1, y_1)$  in the new image. Given  $(cx, cy)$  represents the principle point in either the image, and  $f$  indicates the focal length, we can write the following relationships based on similar triangles:

$$\frac{X}{x_0 - cx} = \frac{Z_0}{f} = \frac{Y}{y_0 - cy} \quad (9)$$

$$\frac{X}{x_1 - cx} = \frac{Z_1}{f} = \frac{Y}{y_1 - cy} \quad (10)$$

Dividing the two equations, we get:

$$a = \frac{x_1 - cx}{x_0 - cx} = \frac{y_1 - cy}{y_0 - cy} = \frac{Z_0}{Z_1} \quad (11)$$

Based on the derived formula, a new depth image can be simply generated via randomly sampling  $a$ , and mapping the area defined by the original four image corners to the new locations in the new image. Meanwhile, the depth values recorded at the new image, and the associated 2D and 3D human part labels can be directly calculated. In our experiments, we sample  $a$  from 0.7 to 1.7 to augment the training data such that the trained model can handle a broader range of observed scale of objects. It is worth mentioning that the depth augmentation method can not simulate the invisible areas from a different camera location, such that the augmented depth data can not fully represent the quality of real captured data.

## B Multi-Person Data Augmentation

Multi-person Data Augmentation is enabled by the training data collected in KD3DH dataset. In the training set, a human subject is recorded at four different locations relative to the camera plus a set of free-style movements, as shown in Figure 9 (top). Besides labels of human joints, foreground human masks are also provided in the training set. Such setup enables background and multi-person augmentation methods. Specifically, given a set of pure background images, as shown in the first examples in Figure 9 (bottom), a human segment from the training set can be used to simply override the pixels with the same region, that leads to a background augmented image, as shown in Figure 8 (Top). Similarly, human segments from different recording locations can be superimposed on random background images following z-buffer rule to compose multi-person augmented images, as shown in Figure 8 (Bottom).

There are a few heuristics associated with the simple augmentation worth to discuss. First, we include no more than two people in the multi-person augmentation with an assumption that inter-person occlusions between two bodies can well represent the inter-person occlusions between more bodies. Second, the straight-forward composition does not consider

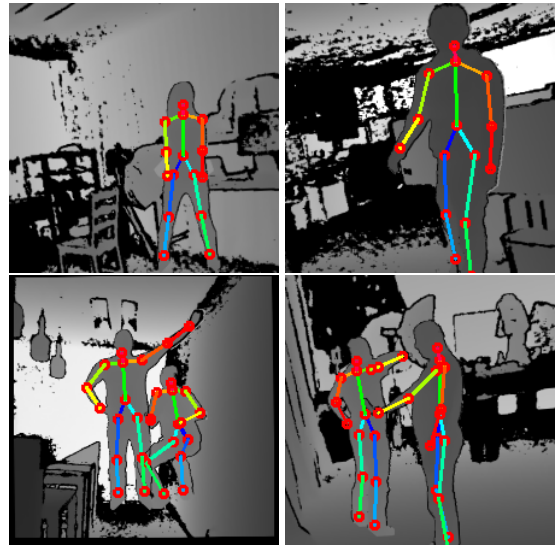


Figure 8: **Augmented training samples.** (Top) Single-person training samples augmented with a random background scene. (Bottom) Augmented multi-person training sample composed from multiple single-person training samples and a random background scene.

scene geometry, such that some generated cases could appear unrealistic. The conflict to the scene geometry is not considered as a serious issue in training, because all the pipelines focus on convolutional layers, such that the learning only depends on the local context between a body part and the background in its vicinity rather than the whole scene. Finally, there are sensor artifacts around each human segment that can not be perfectly removed. This issue indeed affects the generalization capability of a trained model to the real data: a occluded part from the augmented data is still roughly visible because of the black margin around the segment, however an occluded part appears truly invisible in real data.

## C Detailed Running Speed Analysis

Besides FPS, a few more metrics are included to provide a comprehensive understanding of each method’s efficiency. First, the computation complexity of a network is measured in **MACs (G)**, which directly relates to the network inference time. Second, a method’s average running time on an image including a single person (**SP**) is reported in milliseconds per image (ms). This metric considers not only network inference time, but also the essential preprocess to provide bounding boxes or the post-process to extract human poses. Third, a method’s average running time on images including multiple people (**MP**) is similarly reported in milliseconds per image (ms). Finally, a method’s average running speed on images including multiple person is measured by fps which is equivalent to the metric in ms per image on MP data. Every method is evaluated in all the metrics as shown in Table 6.

As observed from MAC (G) scores, Yolo-Pose+ has the lightest network, while A2J has significantly higher network complexity compared to others. However, consider pipeline running time, Open-Pose+ is much slower than the others on images including a single people. This indicates that the

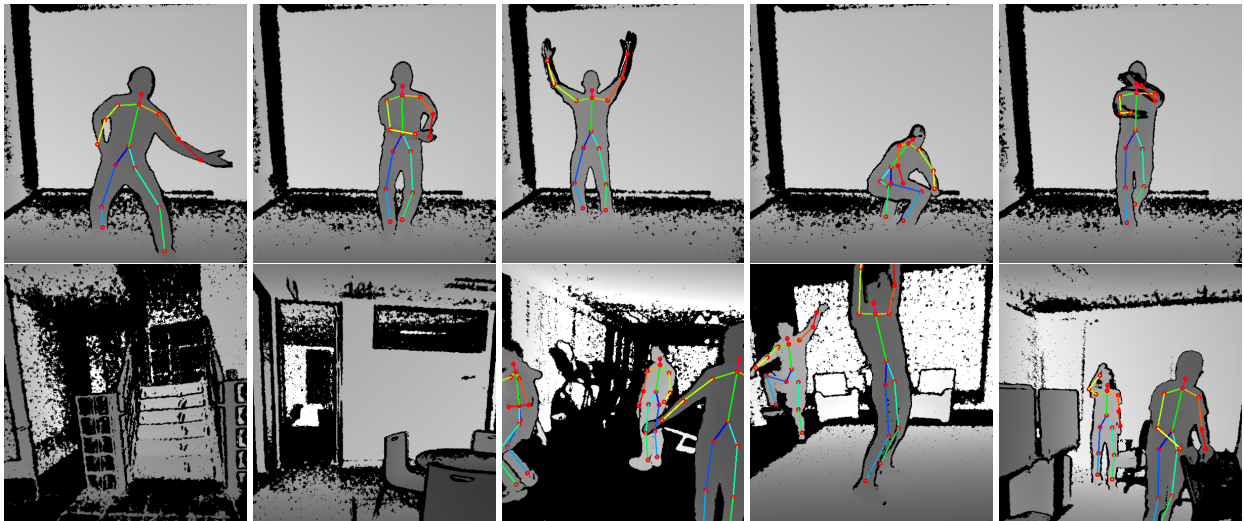


Figure 9: **KD3DH dataset**. (Top) Five single-human examples recorded from different locations from the training set. (Bottom) Two background scenes, and three multi-person testing examples are shown.

part association post-process involved in Open-Pose+ leads to a huge drawback in efficiency. In comparison, PoP-Net involves a much simpler post-process without matching or optimization. Although A2J has a more complex network, it almost has no post-process cost such that its efficiency on a single-person image is even better than Open-Pose+. Finally, as observed from multi-person pipeline running time and speed reported on multi-person testing set from KD3DH, the running speed of A2J drops significantly while the other one-shot methods are not affected. Overall, PoP-Net shows significant advantage in efficiency compared to both A2J and Open-Pose+ for multi-human cases.

challenges.

	Yolo-Pose+	Open-Pose+	A2J	PoP-Net
MACs(G)	4.4	6.7	16.6	6.2
SP (ms)	4.5	20	14	11
MP (ms)	4.5	21	32	11
MP (fps)	223	48	32	91

Table 6: **Runtime analysis on multi-person data.**

## D Qualitative Comparison on Challenging Cases

In order to demonstrate that PoP-Net achieve the STOA and the proposed KD3DH dataset well represents real-world challenges, we visualize the results of competing methods on a set of challenging cases. As shown in Figure 10, (1) shows one example including a target human captured far beyond the observed scale in the training data; (2-3) include two examples having severe background occlusion; (5-6) show two examples including multi-person occlusion but within a solvable scope; (7) includes poses not included in the training set. It is observed that the most challenging cases can fail all the considered method, which indicates that a future work has huge room to improve to achieve robust results in real-world



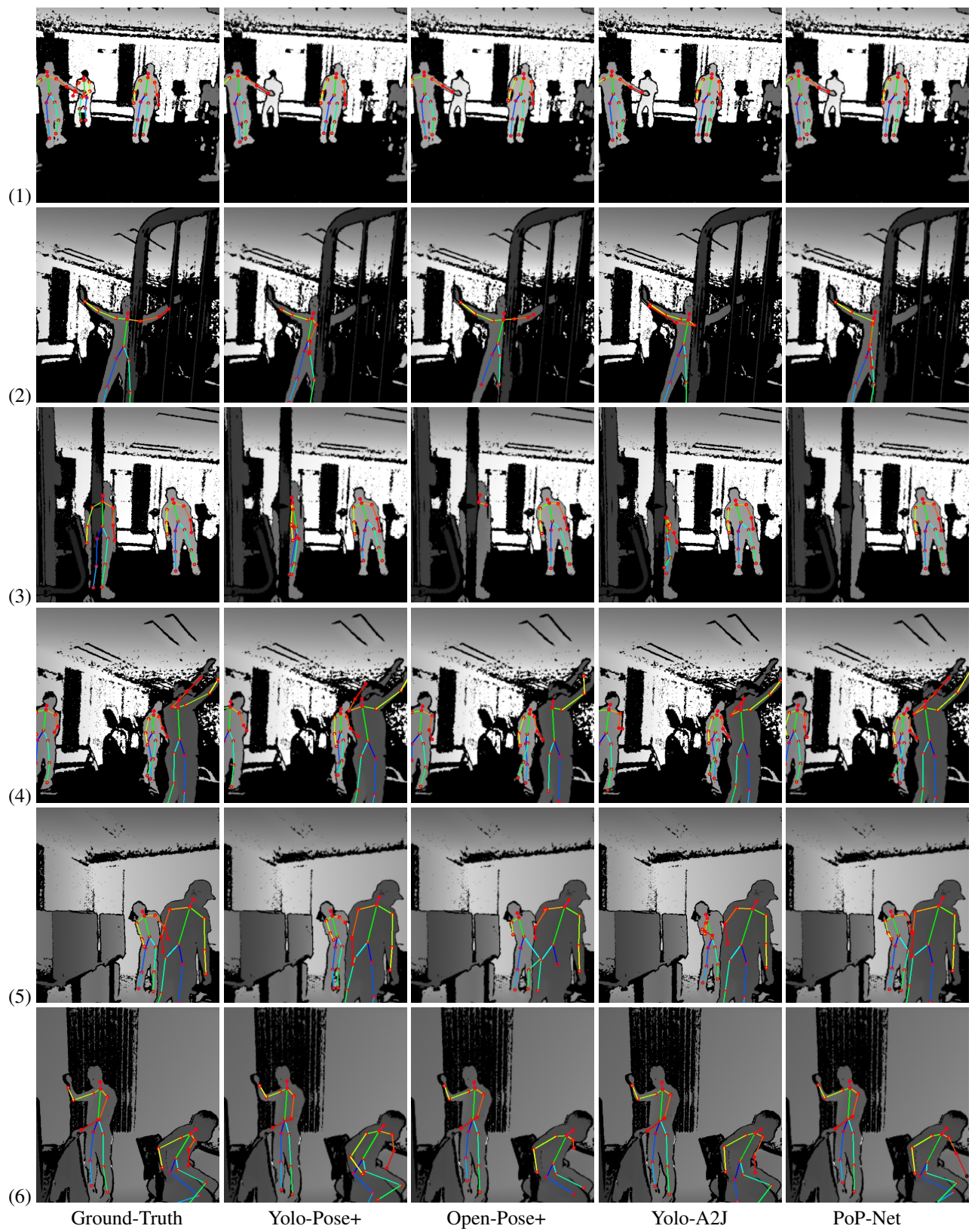


Figure 10: Visual comparison of competing methods on challenging cases.